Daily to annual net primary production in the North Sea determined using autonomous underwater gliders and satellite Earth observation

Benjamin R. Loveday[1,2], Timothy Smyth[1], Anıl Akpinar[3], Tom Hull[4,6], Mark E. Inall[5], Jan Kaiser[6], Bastien Y. Queste[7], Matt Tobermann[5], Charlotte A. J. Williams[3], and Matthew R. Palmer[3]

[1]Plymouth Marine Laboratory, Plymouth, UK
[2]Innoflair UG, Richard-Wagner-Weg 35, Darmstadt, Germany
[3]National Oceanography Centre, Liverpool, UK
[4]Centre for Environment, Fisheries and Aquaculture Science, Lowestoft, UK
[5]Scottish Association of Marine Science, Oban, UK
[6]Centre for Ocean and Atmospheric Sciences, School of Environmental Sciences, University of East Anglia, Norwich, UK
[7]Department of Marine Sciences, University of Gothenburg, Gothenburg, Sweden

Correspondence: Benjamin R. Loveday (ben.loveday@innoflair.com)

Abstract. Shelf-seas play a key role in both the global carbon cycle and coastal marine ecosystems through the drawn-down and fixing of carbon, as measured through phytoplankton net primary production (NPP). Measuring NPP in situ, and extrapolating this to the local, regional and global scale presents challenges however because of limitations with the techniques utilised (e.g. radiocarbon isotopes), data sparsity and the inherent biogeochemical heterogeneity of coastal and open-shelf waters. Here,

5   we introduce a powerful new technique based on the synergistic use of in situ glider profiles and satellite Earth Observation measurements which can be implemented in a real-time or delayed mode system. We apply this system to a fleet of gliders successively deployed over a 19-month time-frame in the North Sea, generating an unprecedented fine scale time-series of NPP in the region (Loveday and Smyth, 2020). At the large-scale, this time-series gives close agreement with existing satellite-based estimates of NPP for the region and previous in situ estimates. What has not been elucidated before is the high-frequency,

10   small-scale, depth-resolved variability associated with bloom phenology, mesoscale phenomena and mixed layer dynamics.

1 Introduction

Our understanding of the global ocean has been transformed over the past two decades by the advent of autonomous observations from gliders and floats (Chai et al., 2020; Roemmich et al., 2019; Mignot et al., 2014; Smith et al., 2011). Such platforms

15   have shown the capability to probe the marine environment at increasingly fine temporal and spatial resolution at local, regional and global scales. Measuring Essential Ocean Variables (EOVs), such as temperature, salinity, chlorophyll-a fluorescence and photosynthetically available radiation (PAR), on these scales has greatly increased our ability to probe the links between physi-

cal systems and primary productivity (Olita et al., 2017; Thomalla et al., 2015). Further, the adoption of autonomous platforms has improved the operational reach of traditional research vessels, which are typically cost and weather limited, and bound to

20 a single point in space and time. This is in contrast to the international Argo float programme which has grown from zero to over 4,000 floats in a little over twenty years. This network now forms a critical part of the Global Ocean Observing System (GOOS) and assimilation of data from individual floats is crucial for global weather forecast models (Le Traon et al., 2019). Currently, Argo floats are operationally constrained to the deep ocean (depth >2 km): gliders have no such constraint, although are around a factor of ten more expensive and require some form of piloting, rendering them less prevalent in the global ocean.

25 The past twenty years have also seen a revolution in space-based sensors, widely and generically termed as satellite Earth observation (SEO). Although SEO gives unprecedented global coverage, infra-red and optical sensors are limited to providing data on the near surface (<1 μm to $\sim$10 m; strictly, the first optical depth) and are therefore unable to resolve variability with depth of key features such as thermoclines and deep-chlorophyll maxima (Gordon and Clark, 1980; Morel and Berthon, 1989; Cullen, 2015). Additionally, passive optical and infra-red SEO coverage is limited by clouds blocking the surface view:

30 strategies to overcome this shortcoming generally involve compositing multiple images of a region, which can lead to the smearing out of sharp boundaries separating physically and biogeochemically distinct water masses at sub-kilometre to tens of kilometres scale resulting in an underestimate of spatial and temporal variability (Carr et al., 2006).

Where SEO missions excel is their ability to provide regional to global estimates of ocean state variables at rates on timescales of days to decades, the latter depending upon the maturity of the measurement time-series. An example of this, and the

35 subject of this manuscript, is net primary production (NPP), the carbon fixed by plants through photosynthesis: the basis of almost all terrestrial and marine food webs. NPP plays a critical role in Earth's climate system by regulating the draw-down of atmospheric carbon dioxide (Parekh et al., 2006) and the air–sea exchange of radiatively important trace gases (Nightingale et al., 2000; Wanninkhof, 1992). SEO NPP algorithms widely estimate that marine phytoplankton fix carbon at a rate of 45–50 Gt a^{-1} (Carr et al., 2006) representing approximately half of all global NPP (Field et al., 1998). In contrast, in situ

40 measurements of NPP in the open ocean are sparse, are generally made in the more clement months of the year, and target interesting features such as upwelling zones (Joint et al., 2002) or seasonal phytoplankton blooms (Robinson et al., 2009). Furthermore, regular fixed-point sampling (Barnes et al., 2015) is difficult to extrapolate due to spatial variability.

Significant improvements in NPP estimates from SEO surface chlorophyll-a concentration ([Chl-a]) fields are possible with simultaneous in situ chlorophyll fluorometry and PAR profiles (Jacox et al., 2015). Hemsley et al. (2015) demonstrated and

45 validated in the North Atlantic, a method for estimating NPP at high vertical and temporal resolution, using glider chlorophyll fluorescence and irradiance profiles. Significantly, it used irradiance to calibrate fluorescence and, therefore, needed no in situ samples for calibration. Hemsley et al. (2015) made possible depth-resolved continuous estimates of NPP over a full seasonal cycle, in all weathers.

In this paper we present a synergistic method, using a combination of in situ glider (Hemsley et al., 2015) and SEO, for

50 estimating NPP at high vertical and temporal resolution. This method is translocatable to any region of the global ocean, and is designed to support processing in delayed (DM) and operational near real-time (NRT) modes. It allows for flexible selection of algorithms to enable and, through the incorporation of SEO data, provides a consistent output despite inconsistent

glider payloads or platform types. We apply this method to an 19-month autonomous glider field campaign in the North Sea, a critical shelf-sea for fisheries with other multiple environmental stressors including eutrophication (Ferreira et al., 2011),

55   deoxygenation (Queste et al., 2016), shipping (Barry et al., 2006) and pollution (Salomons et al., 2012). For the first time we uncover the considerable temporal and spatial variability in NPP, driven by seasonal succession, fronts (Miller, 2009) and topographical features, as well as capturing two winter seasons which are crucial in conditioning the system for the following spring and summer periods.

2 Ingested glider data

60   As part of the Alternative Framework to Assess Marine Ecosystem Functioning in Shelf Seas (AlterEco) project, a sustained presence of autonomous underwater gliders in the North Sea was maintained between November 2017 and May 2019. The programme aimed to keep at least two gliders in the field at all times, to provide measurement redundancy and assist with data validation. All gliders had a basic instrumentation package consisting of Conductivity Temperature Depth (CTD) in order to determine vertical profiles of temperature and salinity, and a Seabird Scientific ECO-puck for fluorescence and back-scattering

65   measurement. The data set presented here is confined to only those gliders with ECO-pucks configured for chlorophyll fluorescence measurement. Beyond this, the payload of each individual glider differed depending on the requirements of the individual mission goals (figure 1a). Throughout the AlterEco campaign, the gliders occupied a consistent East-West (1.5° - 2.5°E, along 56.1°N) and North-South (55.2° - 56.2°N, along 2°E) transect (see figure 1b), with the southern extent of the latter venturing on to Dogger Bank.

70   AlterEco glider missions are grouped in seven deployments[1], outlined in table 1. The glider data for these deployments is available from the British Oceanographic Data Centre (BODC) at https://www.bodc.ac.uk/data/bodc_database/gliders/. The data is supplied in the Everyone's Gliding Observatories (EGO) format [2], which aggregates all profiles from a single glider mission into one NetCDF file.

3 Method

75 ### 3.1 Overview of the NPP processor

The NPP processor comprises a set of Python-based routines that manage the ingestion, quality control, correction, and pre- and post-processing of autonomous underwater glider profiles, as well as interfaces with external routines to calculate spectral PAR (Gregg and Carder, 1990) and NPP itself (Morel, 1991), which are implemented in the C programming language. Figure 2 shows a detailed flow diagram for the various processing stages. The processor supports multiple approaches to NPP

80   calculation, depending on the availability of glider-based optical sensor data.

---

[1]doi; 10.5285/b57d215e-065f-7f81-e053-6c86abc01a82 and 10.5285/86429662-97b8-74fa-e053-6c86abc0a97c
[2]http://dx.doi.org/10.25607/OBP-768)

At its heart, the algorithms used to calculate NPP are as described in Hemsley et al. (2015): these in turn draw heavily upon the spectral light NPP formulation of Morel (1991). However, this method is modified to cater for fluorescence quenching and light attenuation in shelf-seas, as opposed to the open ocean (as discussed in section 3.4). For the purposes of determining NPP, the optimal glider instrument payload consisted of (in order of importance) chlorophyll-a fluorescence, PAR and optical

85 backscatter (Hemsley et al., 2015). Figure 1a shows that only four missions (497, 454, 499 and 517) had the full complement of required sensors, which necessitated modifications to the Hemsley et al. (2015) algorithms (see table 1).

3.2 Data acquisition and staging

The processing chain was designed to accommodate either near real-time mode (NRT) or delayed-time mode (DM) implementations, and as such ingests glider data either as individual NetCDF profiles as they become available (in NRT) or in EGO

90 NetCDF format (in DM). The data set described here is processed in DM. Files may be ingested locally, or auto-downloaded from a remote FTP repository on a user determined schedule. All ingested source files are stored in an initial deployment directory, and catalogued in a centralised SQLite database. This non-destructive approach supports the continual updating of the glider record from a remote catalogue in the NRT case, while preventing replication. The database monitors, records and manages all subsequent stages of the processor.

95 NPP calculations are performed on a profile-by-profile basis. Glider data typically consists of both downward (dive) and upward (climb) components in a single file, which in our processing framework represents two profiles. If a pre-existing profile designation is provided, as is usually the case in EGO data, this is used to split the source data into profiles. If no designation is provided, the ingested data is split into single files according to the turning points in the smoothed depth record. Smoothing is performed using a 5th order Savitzky–Golay filter, with a nominal window of 151 points. Individual profiles are then stored

100 in the staging directory for future use.

3.3 Constructing Earth Observation trajectories

Due to trade offs necessary to achieve the multiple mission priorities of the AlterEco programme, not all gliders were able to accommodate PAR sensors. Here, when required, SEO-based PAR data is used in lieu of in situ measurements. This increases both the flexibility and utility of the method for the operational oceanography community, allowing it to be applied to glider data

105 where only in situ chlorophyll-a fluorescence is available. In addition, SEO and reanalysis data is used to provide information on the prevailing atmospheric and marine conditions during each glider mission. A list of SEO and reanalysis data sources, and the variables that are extracted and/or derived can be found in table 2 and in figure 2.

When a glider mission is updated (e.g. a new profile is added in NRT mode), the processor calculates the new temporal and spatial extents of the mission. Using these extents, the processor gathers the required SEO and reanalysis data from the specified

110 source, concatenates the retrieved catalogue in time and trims the spatial coverage to produce a 'data cube' that matches the glider mission extents. The spatial trimming is performed remotely, on the server side, if the data service in use allows this capability, reducing data transfer costs and time. In NRT mode, new data is added to extend the cube as required, without the need to download the entire catalogue once again (e.g. via the concatenation of new time slices to the existing local record).

This operation is performed for all variables, for all gliders, irrespective of whether they have the relevant in situ measurement,
115   allowing for the continual validation of the use of SEO and reanalysis data as a substitute.

Once the data cube has been constructed, the average time and location of each profile are extracted and concatenated into
a one-dimensional time series of the glider trajectory. Bi-linear interpolation is then used to retrieve the corresponding SEO
and reanalysis data from the relevant data cube, resulting in an SEO-trajectory file for each variable, with a value for each
profile. During construction, the cube is both spatially and temporally 'padded' to eliminate 'edge effects' associated with
120   interpolation.

3.3.1   Treatment of PAR data

SEO-based broadband PAR values (E_d), defined as the average PAR value between 400 nm to 700 nm, are derived from
MODIS daily average values, measured in mol m^{-2} d^{-1} (Frouin et al., 1989) (see table 2). Instantaneous values of broadband
PAR, corresponding to the glider measurement times, are derived from the average values as follows. The light distribution
125   is modelled as a sine curve between dawn (T = 0) and dusk (T = π). The amplitude of this curve is determined such that the
integrated value below it matches that of the daily average. The instantaneous value is then extracted by interpolating the curve
at the glider measurement time, and converted to W m^{-2}.

3.4   Pre-processing

The pre-processing step consolidates the glider and SEO-based data on a profile-by-profile basis, performs quality control
130   procedures and selects the relevant variables for NPP calculations depending on availability (figure 2). Sporadic missing values
are common in in situ data. Where possible, linear interpolation is used to fill these gaps in the positional, depth and pressure
data. If interpolation is not possible, the profile is discarded and no further processing takes place.

Following this, and where not provided directly, conservative temperature and absolute salinity are calculated from the glider
CTD record using the TEOS-10 Python GSW toolbox [3]. Mixed layer depth (MLD) is then calculated from the density gradient
135   according to Holte and Talley (2009). If the MLD calculation fails, the MLD from the previous profile is used. The MLD is
prevented from being shallower than 5 m, as depths shallower that this are typically poorly sampled by a glider. Once the
physical variables are processed, the PAR and [Chl-a] profiles are assessed, along with the back-scattering data, if present.

PAR data delivered in raw counts is corrected to W m^{-2} using the calibration coefficients specific to the sensor. The in situ
[Chl-a] data is similarly treated. In the latter case, [Chl-a] data is discarded where the calibrated value exceeds $1e^5$ mg m^{-3}.
140   In the case of DM processing, post mission calibration factors can also optionally be applied, though none were applied in this
case.

---

[3] https://teos-10.github.io/GSW-Python/

3.4.1 Determining the PAR profile

PAR sensors do not always acquire at the same sampling rate as the glider CTD sensor. Consequently, where it is available in situ PAR data for a given profile is interpolated onto the glider depth record prior to further processing. The decision point for
145   the use of glider or SEO-based broadband PAR is made as follows;

- Where a profile falls during the day-time and glider E_d is available, this is used by default (though the use of SEO-PAR can be forced, to permit validation). K_{dPAR} is calculated from the linear regression of the logged PAR values with depth. The regression is weighted by the square-root of the magnitude of the logged PAR values, emphasising the effect of the surface layers. E_d at depth is then projected to the surface using the K_{dPAR} value, giving sub-surface broadband PAR
150   (E_o^-). Broadband PAR at at the surface (or just above) (E_o^+) is derived from E_o^- using the method described in Hemsley et al. (2015). Fresnel reflectance is calculated using the wind speed, relative humidity and mean sea level pressure derived from the SEO trajectory files.

- Where glider PAR is not available SEO-based surface broadband PAR (E_o^+) is substituted. E_o^- is calculated as described in the previous step. SEO $\overline{K_{dPAR}}$, calculated from SEO $\overline{K_{d490}}$ Saulquin et al. (2013), is then used to project broadband
155   PAR into the subsurface across the glider depth record.

- Where SEO K_{d490} is not available, $\overline{K_{dPAR}}$ is calculated according to equation 1 (Saulquin et al. (2013)), where PAR(Z_{eu}) is assumed to be 1% of PAR(0), and the euphotic depth (Z_{eu}) is determined from the maximum in situ [Chl-a] above the MLD, according to equation 2 Lee et al. (2007).

$$\overline{K_{dPAR}} = \frac{(ln(PAR(0)) - ln(PAR(Z_{eu})))}{Z_{eu}} \tag{1}$$

160   $$Z_{eu} = 34.0 \times CHL^{-0.39} \tag{2}$$

The PAR record is labelled as bad, and is not processed, in the case of i) night-time profiles, ii) substantial gaps in the [Chl-a] data, or iii) where the glider is within 5 m of the bathymetry depth, as interpolated from the GEBCO 15 arc-second gridded product [4]. The latter criteria prevents the glider from deriving NPP estimates from [Chl-a] readings that may have been gathered at depths where particle re-suspension in likely to make them unreliable. Euphotic depth (Z_{eu}: defined as the 1% of
165   the surface light depth) is subsequently calculated for all good profiles, and is selectively used in the correction of the [Chl-a] profile.

To validate this approach, Figure 3 a) and b) compares the in situ and SEO-based E_d estimates for gliders 517 (Cabot) and 454 (Cabot), respectively. For both missions the SEO surface PAR around solar noon under-predicts the surface PAR

---

[4]https://www.gebco.net/data_and_products/gridded_bathymetry_data/

reconstructed from the glider profiles by typically ∼50 W m^{-2}. In addition, the SEO-based values do not take account of the

170   instantaneous cloud conditions and, correspondingly, the standard deviation in the surface PAR time series is lower. However, the SEO-based interpolation method gives an accurate facsimile of the daily PAR cycle, with a mean $\bar{E}_o^+$ that falls within 7% of the in situ broadband value. This error value that is comparable with the 5% "in air" performance of the in situ PAR sensor itself [5].

3.4.2   Using the optical backscatter profile

175   Where available, optical backscattering measurements (b_{bp}) may be used to correct the surface chlorophyll fluorescence profile for near-surface quenching (Hemsley et al., 2015). The backscattering data is initially passed through a 7-point running minimum filter to remove spikes (Thomalla et al., 2018). Negative values are removed and the scattering profile is subsequently interpolated onto the glider depth record.

3.4.3   Quality control and quenching correction of the chlorophyll fluorescence profile

180   The glider chlorophyll data is initially screened for erroneous values, with measurements of [Chl-a] < 0.0 mg m^{-3} discarded. To account for bio-fouling, the record is also discarded where there is a consistent "step change" of > 5 mg m^{-3} in [Chl-a] at depths below both the MLD and Z_{eu}, as compared with the initial deployment value. As with the treatment of the PAR data, the [Chl-a] is then interpolated onto the glider depth record on a profile-by-profile basis. Where the interpolation fails due to lack of data, the entire profile is discarded and no NPP calculation is performed.

185   Fluorescence quenching in phytoplankton is caused by a variety of physiological acclimation mechanisms in order to avoid photo-damage under excessive irradiance (Kiefer, 1973). This effect typically manifests as a depression of the fluorescence signal in the surface waters during daylight, and particularly around solar noon when the downwelling irradiance is at a maximum (Xing et al., 2012; Biermann et al., 2015). Multiple approaches to quenching correction have been proposed, e.g. Xing et al. (2012); Biermann et al. (2015); Hemsley et al. (2015); Swart et al. (2015); Thomalla et al. (2018). The applicability

190   of these methods depends on the region being studied and the availability of optical backscattering data. Four methods are tested for this data set;

  – The Xing et al. (2012) method; where the maximum [Chl-a] measured in the mixed layer is projected to the surface for day-time profiles. This method can be used in either DM or NRT cases.

  – The Biermann et al. (2015) method; where the maximum [Chl-a] measured above the euphotic depth is projected to the

195   surface for day-time profiles. This method can be used in either DM or NRT cases.

  – The Swart et al. (2015) method; where the optical backscattering signal above the euphotic depth is used to correct the corresponding [Chl-a] on a profile by profile basis. This method can be used in either DM or NRT cases.

---

[5]https://www.seabird.com/asset-get.download.jsa?id=54627862114

– The Hemsley et al. (2015) method; where, again, the optical backscattering signal is used to correct the corresponding [Chl-a] using the night-time relationship with backscattering, as measured across the entire glider mission. This method can be used in DM cases, only.

Due to the lack of available light during night-time sampling, [Chl-a] profiles remain unquenched. The extensive variability in shelf-seas makes direct correction of day-time profiles to their nearest night-time counterpart challenging (Carberry et al., 2019). However, when quenching is appropriately accounted for day-time [Chl-a] profiles should, in the aggregate, approximate their night-time counterparts. Figure 4 compares the histogram distribution of night-time and day-time [Chl-a] profiles for three tested methods across the entire gliders 517 (Cabot) and 454 (Cabot) missions. Optical complexity in coastal waters, associated with the presence of sediment, undermines the relationships between [Chl-a] and the backscattering record. Consequently, while it may perform well in the open ocean, the quenching correction method described by Hemsley et al. (2015) performs poorly in this case. The Swart et al. (2015) method (not shown) is similarly unsuitable.

The Xing et al. (2012) method clearly outperforms the other methods tested, and is used to process all the gliders deployed during the AlterEco programme. Its strong performance is ascribed to its ability to appropriately capture the regional seasonal interplay between the MLD and euphotic depth in the shelf seas. As shown in figure 5, the MLD sits above the euphotic depth during spring. This allows for the establishment of a deep chlorophyll maxima (DCM) (see figure 6), which is particularly important for NPP in this region (Fernand et al., 2013). In this case, quenching corrections using euphotic depth as a maximum depth limit (e.g. (Biermann et al., 2015)) over-correct as they tend to encapsulate the DCM in the quenching correction process, extrapolating erroneously high [Chl-a] to the surface.

3.5 Calculating and scaling the spectral irradiance profile

Once the pre-processing stages have been completed for all available glider profiles (figure 2) spectral E_d profiles are calculated for each using the solar irradiance model described by Gregg and Carder (1990). To account for local meteorological conditions, the model runs using the $[O_3]$, cloud cover, wind speed, relative humidity and total column water vapour parameters for each profile, stored in the relevant trajectory file (Table 2). These spectral E_d values calculated from the model are scaled such that their integrated value between 400 nm and 700 nm matches the corresponding E_o^+ measurements provided by the glider or SEO data sources (see section 3.4.1). This scaling correction accounts for instantaneous sky conditions associated with each profile.

3.6 Implementing chlorophyll-a scaling

The work by Hemsley et al. (2015) implemented a novel methodology to exploit the relationship between PAR and [Chl-a] to account for changes in the apparent fluorescence to chlorophyll calibration, brought about by phytoplankton community succession. This approach allows dynamic changes to the calibration, and reduces the need for in-field calibration, which is difficult, if not impossible to implement, especially in the near real-time case. However, this method is based on an in water

model suitable for Case-1 waters (Carr, 1986), with the non-water component of light attenuation ascribed to [Chl-a] only
230 (Morel and Maritorena, 2001).

The processor retains the ability to implement this method, as detailed extensively in Hemsley et al. (2015) and represented in Figure 2 by the "Case 1" decision box. However, the optically complex waters of the shelf-seas are rich in sediment, and do not conform to the Case-1 paradigm. Implementation of a spectral irradiance model more suitable to the region requires the consistent deployment of in situ PAR and back-scattering sensors that is not available across the AlterEco programme.
235 Consequently, no PAR-based scaling of the [Chl-a] profiles is performed for this data set. This caveat is further discussed in section 5.4.

3.7 Calculating NPP

Net primary production is calculated from the corrected [Chl-a] and depth profiles and spectral downwelling PAR for each profile using the Morel (1991) model, as presented in Hemsley et al. (2015) and shown in equation 3. The model calculates
240 NPP through a triple integral across day length (L), depth ($D_1 = 0$, $D_2 = Z_{eu}$) and wavelength (λ_1 = 400 nm, λ_2 = 700 nm). The absorption cross section per unit of chlorophyll (a^* [m^{-1}]) and net growth rate (ϕ_μ [mol(carbon) mol(quanta)$^{-1}$]) are parameterised as in (Morel, 1991).

$$NPP = 12 \int\limits_{0}^{L} \int\limits_{D_1}^{D_2} \int\limits_{\lambda_1}^{\lambda_2} [Chl\text{-}a](Z) E_d(t,Z,\lambda) a^*(\lambda) \phi_\mu(t,Z,\lambda) d\lambda dZ dt \tag{3}$$

NPP estimates, in units of carbon flux (mg m^{-3} d^{-1}), are calculated for all uncorrected and corrected [Chl-a] profiles, using
245 the per-profile average time and position for each. The piece-wise measurements are integrated from the 1% light level (as determined by the model) to the surface to give a final estimate of depth integrated primary productivity in carbon flux of mg m^{-2} d^{-1}.

Figure 7 allows a comparison of using SEO-based PAR in the calculation of spectral E_d and, subsequently NPP, in contrast to using in situ PAR. SEO-based PAR is shown to function as a suitable proxy in this method, remaining highly correlated with
250 its in situ counterpart, with mean values that are within 2% of the target estimate.

When combined, the NPP times series derived from the AlterEco glider deployments spans a 19-month period, as shown in figure 8. Two peaks are captured in April/May 2018 and April 2019, corresponding with the timing of the regional spring bloom, and with the latter event significantly more intense. Independent [Chl-a] estimates, derived from v4.2 of the ESA Ocean Colour Climate Change Initative (OC-CCI) data set (Sathyendranath et al., 2019), indicate that the 2018 spring bloom
255 was relatively intense, suggesting that 494 (Stella) failed to fully capture this event. As expected, NPP drops to near zero in the winter months, when light availability becomes limiting. Black traces, indicating NPP estimates derived from in situ PAR sensors, compare well with their coloured (SEO derived) counterparts in all cases. However, the divergence between the signals recorded by the concurrently deployed gliders 455 (Orca), 497 (Humpback) and 454 (Cabot) strongly suggests the presence of significant spatial heterogeneity in the region north of the Dogger Bank.

4 Data provenance and structure

The complete finalised data set consists of 13 netCDF files, in EGO format. Each netCDF file corresponds to a single glider mission. The data covers a region spanning a longitude of -1.497^o W to 2.577^o E, a latitude of 51.005^o N to 58.669^o N and a time period of 15/11/2017 to 28/05/2019. During deployment 481 (Kelvin) the glider remained at the surface from 21/11/2018 to 02/12/2018 and did not acquire [Chl-a] data and so no NPP was calculated for this period. No other glider was deployed during this time, resulting in a single 10 day gap in the record. Each EGO data file, contains the variables listed in table 3.

Responsibility for maintaining the data set lies with Plymouth Marine Laboratory, the provenance authority for the final output. No updates of the data set are expected. The data set is stored in the British Oceanographic Data Centre (BODC) archive, and has the following digital object identifier: https://www.bodc.ac.uk/data/published_data_library/catalogue/10.5285/b58e83f0-d8f3-4a83-e053-6c86abc0bbb5/.

5 Data validity

5.1 Fluorescence quenching validity

In order to quantify the efficacy of the various quenching correction algorithms upon the chlorophyll fluorescence profiles, a comparison was made between the day-time (quenched) and night-time (not quenched) [Chl-a] over the top 20m of the water column. This comparison assumes that there is little change in the vertical profile of [Chl-a] in a 24 hour period: this is obviously a simplification as there will be changes due to (1) bloom growth or decay and (2) spatial variability. Figure 4 shows that the major discrepancy between the night-time and the uncorrected day-time [Chl-a] profiles, for glider 454 (Cabot: see Figure 1 and Table 1), is when the integrated [Chl-a] in the top 20 m exceeds 5 mg m^{-2} and is less than $\sim$ 12 mg m^{-2}. The percentage variance between day-time and night-time cases uncorrected cases is 91.0% with a significance p value of <0.01. The Xing et al. (2012) method (Figure 4) clearly outperforms the other correction methods tested in this case (r^2 = 97.8% p<0.01; cf. Hemsley et al. (2015) r^2 = 32.8% p<0.01 and; Biermann et al. (2015) r^2 = 0.2% p=0.81). Similar results were obtained for glider 517 (Cabot: see Figure 1 and Table 1) with for uncorrected (r^2 = 92.7% p<0.01) and Xing et al. (2012) (r^2 = 97.8% p<0.01); the other two algorithms interchanged their ranking however with Biermann et al. (2015) (r^2 = 73.3% p<0.01) and Hemsley et al. (2015) (r^2 = 26.2% p<0.01).

Figure 6 shows the corrected [Chl-a] profiles for glider 454 (Cabot). The corrected time-series shows a gradual deepening of the DCM over the three month mission from around 25 m in mid-May (2018) to 40 m in mid-August. During this period there is also a clear reduction in the peak [Chl-a]: >3 mg m^{-3} at the start of the mission, $\sim$1 mg m^{-3} towards the end. The transects on and off Dogger Bank (depths shoaling to around 40 m) are clearly correlated with a shoaling of the euphotic depths from $\sim$ 30 m on the Bank to $\sim$ 50 m off the Bank. Changes in the MLD are less pronounced, apart from a deepening between June 18 and 22 2018, and a rapid shoaling from 30 to 18 m around 24 June 2018. Meteorologically, June 2018 was characterised by relatively slack pressure gradient (light winds) until a brief three day period of stronger north or north-westerly winds on 19/22 June which corresponds to the episodic deepening of the MLD in this period.

5.2 Comparison with historical measurements in the North Sea

Two distinct advantages of gliders are that they sample flexibly, in terms of horizontal space and depth, and they can gather
data at high frequency. As there are no pre-existing measurements of NPP in the North Sea with comparable frequency, here
295 we compare our results with available estimates of annual mean productivity. Table 4 summarises the monthly and annual
NPP estimates across all campaigns. The annual cycle and mean annual NPP rate agrees well with contemporaneous values
interpolated from the monthly mean OC-CCI based NPP climatology for 1998-2018 (Kulk et al., 2020). It is notable that, while
still within one standard deviation, the April NPP peak in the glider data is somewhat lower than its OC-CCI counterpart, likely
as a result of the low signal recorded by 494 (Stella) over this period in 2019. The glider-based NPP signal peaks at a time
300 consistent with remote sensing estimates.

The glider-based annual mean NPP value 98 gC m^{-2}a^{-1} is comparable with the 119 gC m^{-2}a^{-1} measured through extensive
surveys carried out over ICES Region 7 (north of Dogger Bank) by Joint and Pomroy (1993), as well as with observation based
estimates of 125 gC m^{-2}a^{-1} for the northern North Sea (van Beusekom and Diel-Christiansen, 1994). The glider measurements
are similarly consistent with NPP estimates derived from models; with Varela et al. (1995) recording 130 gC m^{-2}a^{-1} for ICES
305 Region 7 (as used by Joint and Pomroy (1993)), Moll (1998) simulating 119 gC m^{-2}a^{-1} across the northern North Sea and
Zhao et al. (2019) reporting 82.6 - 118.8 gC m^{-2}a^{-1} for the central and northern North Sea in their tidal simulations.

Alongside NPP, Varela et al. (1995) provides estimates of gross primary production (GPP). In the northern North Sea (ICES
region 4), an NPP of 149 gC m^{-2}a^{-1} is associated with a GPP of 314 gC m^{-2}a^{-1}. Similar modification of the glider based
NPP measurements to a GPP estimates suggests an approximate value of ∼200 gC m^{-2}a^{-1}. This compares favourably with the
310 measurements of Capuzzo et al. (2018), who reported an annual mean gross production of 200±15 gC m^{-2}a^{-1} in seasonally
stratified regions from 1998 to 2013 (including Dogger Bank).

5.3 Value and utility

Primary production is highly variable on short temporal and spatial scales. The impact of the mesoscale variability associated
with fronts (Olita et al., 2017; Taylor and Ferrari, 2011) and eddies (Hansen et al., 2010; Hu et al., 2014) can be extensive. High
315 frequency changes in tidal phase (Zhao et al., 2019), sky conditions and the local wave field (Reed et al., 2011) can also exert a
strong influence. To monitor the impact of these processes in highly productive shelf seas, it is desirable to continually sample
key regions using technologies that support adaptive sampling strategies. Autonomous underwater vehicles (AUVs), such as
gliders, offer one such approach to this problem, offering persistent monitoring of shelf sea biogeochemistry (Chai et al., 2020;
Liblik et al., 2016) and informing regional model assimilation strategies (Skákala et al., 2021).
320 This data set presents the first intra-annual, glider-based in situ NPP time series for the North Sea, that is able to address
questions pertaining to biophysical interactions on a high-frequency basis. From figure 8 it is clear that the NPP signal is
modulated at multiple frequencies within individual deployments, and substantial spatial heterogeneity exists between co-
deployments (e.g 455 (Orca) and 454 (Cabot)). Further analysis of this data set should give insight into the physical processes
that contribute to this variability.

325 When deployed with multiple mission goals in mind, glider payload space typically comes at a premium. Most notable in this case, is the effect on the deployment of PAR sensors, which are present on less than 50% of missions. However, adaptation of previous methodology to accommodate SEO based PAR estimates has been shown to be feasible. Combining SEO surface data with AUV profiles also presents interesting options for reconstructing subsurface fields. Machine learning methods have demonstrated the feasibility of combining SEO surface fields with in situ profile to render a three dimensional picture of ocean

330 biogeochemical properties (Sauzède et al., 2015, 2016). The data set presented here would be well suited for application of such methods to evaluate and further extend coverage of NPP data in the global ocean.

The processing method developed here allows for glider-based NPP to be calculated in a much broader array of cases. While in DM it can replicate the approach of Hemsley et al. (2015), the inclusion of differing quenching algorithms promotes application to different regions and/or different sensor loads (e.g. those without back-scattering). The flexible inclusion of SEO

335 data in lieu of in situ PAR measurements expands this utility even further, allowing NPP calculations from gliders with a more limited array of sensors without substantial loss of accuracy (Figure 7). Finally, the ability to support NRT ingestion of glider data allows for NPP calculation in an operational setting.

5.4 Limitations

PAR, when spectrally decomposed, can be used to provide a calibration of the [Chl-a] fluorometer (Hemsley et al., 2015).

340 Although the fluorometer calibration may be accurate at the start of an individual mission, calibration using nearby discrete [Chl-a] samples at launch and retrieval of the glider may lead to a false sense of security, particularly in areas of high heterogeneity, such as experienced during this study. Hemsley et al. (2015) showed that within mission variability in the correction factor is possible due to changes in phytoplankton community structure. However, the model previously proposed is suitable for case-1 waters only, and does not account for absorption and scattering by CDOM and sediment, respectively, and so no dynamic

345 calibration is applied here. The strong agreement between AlterEco glider NPP measurements and both satellite and historical in situ estimates (see section 5.2) underlines the validity of the data set, and future work will consider the incorporation of a model to cater for more complex waters, where glider payload allows.

While the quenching correction method of Xing et al. (2012) proved most appropriate in this case, this result should not be a considered a general solution. This rationale underpins the decision to incorporate multiple methods to correct near sur-

350 face fluorescence, however, the eventual method chosen is limited by the sensors deployed, most notably the availability of backscattering data (Figure 1). The availability of back-scattering data allows for the a wider selection of correction methodologies in both DM (Thomalla et al., 2018; Hemsley et al., 2015) and NRT (Swart et al., 2015) processing. In addition, its inclusion is essential to constructing a complex water model, as discussed earlier in this section.

For long duration missions (i.e. more than a few days) bio-fouling of sensors mounted on gliders can affect data quality.

355 Unlike Argo floats, which typically park at depths well below the euphotic zone (∼1 km), for 10 days, gliders spend a greater portion of their time in the photic zone, allowing the build-up of a bacterial substrate and then algal colonisation. Despite many strategies to mitigate bio-fouling (copper covered sensors, bio-wipers), it is impossible to completely eradicate it currently, and even predicting its onset is problematic. Anecdotally on moorings situated in the western English Channel (Smyth et al., 2010a,

b), bio-fouling has been observed to take several months to colonise sensors, and then following cleaning, has only taken a few
360   weeks re-emerge. Best efforts have been made to truncate the glider [Chl-a] record where bio-fouling appears evident (section
3.4.3).

6   Conclusions

This paper discusses the generation of an 19-month, near-continuous glider-based data set of net primary production in the
North Sea; the first of its kind for the region. The methodology used to derive this time-series is discussed in detail, with
365   specific focus on the approaches taken to account for fluorescence quenching and the use of SEO-based PAR data in lieu
of in situ sensors. While, in this case, pre-processed glider data from the AlterEco programme serves as a starting point,
consideration is also given to adaptation of the method for NRT and operational use. Although limitations in the approach used
are discussed, especially in regard to the feasibility of dynamic calibration and effects of biofouling, the results show strong
agreement with previous studies as well satellite derived estimates and the results of biogeochemical model simulations. They
370   present a unique, depth-resolved picture of the high-frequency variability and spatial heterogeneity present in the production in
region and highlight the advantages of using autonomous systems to persistently monitor the shelf-seas, especially in tandem
with remote sensing based approaches. The newly developed processing approach also has implications for the development of
a PP indicator (e.g. through the Marine Strategic Framework Directive food web descriptor), overcoming some of the temporal
and spatial sampling limitations that have historically undermined its inclusion in assessments, relegating its listing to candidate
375   only.

7   Code and data availability

The data is made available via the British Oceanographic Data Centre (BODC), via doi:10/fm39. For full details, please see
Loveday and Smyth (2020). Access to the code for the primary productivity processor is available, via GitLab, on request to
the lead author.

380   *Author contributions.* Ben Loveday and Tim Smyth developed the methodological approach and led writing of the manuscript. Ben Loveday
built the processing system and generated the resulting data set. The remaining authors are responsible for the glider deployments, the
provision of supporting data sets and calibration information, and for providing methodological input in the manuscript.

Competing interests. The authors declare that they have no competing interests.

Acknowledgements. This work was funded by the NERC Alternative Framework to Assess Marine Ecosystem Functioning in Shelf Seas
385 (AlterEco) programme under grant numbers NE/P013899/1, NE/P013910/1 and NE/P013902/1. The authors thank Emma Slater for managing data ingestion and hosting at BODC; Dr Thomas Jackson at Plymouth Marine Laboratory for providing the OC-CCI data used in table 4, and Dr Hayley Evers-King for proof reading and comments on the manuscript narrative.

References

Barnes, M. K., Tilstone, G. H., Suggett, D. J., Widdicombe, C. E., Bruun, J., Martinez-Vicente, V., and Smyth, T. J.: Temporal variability in total, micro-and nano-phytoplankton primary production at a coastal site in the western English Channel, Progress in Oceanography, 137, 470–483, 2015.

Barry, M., Elema, I., and Van Der Molen, P.: Governing the North Sea in the Netherlands, Administering Marine Spaces: International Issues, p. 64, 2006.

Biermann, L., Guinet, C., Bester, M., Brierley, A., and Boehme, L.: An alternative method for correcting fluorescence quenching, Ocean Science, 11, 83–91, 2015.

Capuzzo, E., Lynam, C. P., Barry, J., Stephens, D., Forster, R. M., Greenwood, N., McQuatters-Gollop, A., Silva, T., van Leeuwen, S. M., and Engelhard, G. H.: A decline in primary production in the North Sea over 25 years, associated with reductions in zooplankton abundance and fish stock recruitment, Global Change Biology, 24, e352–e364, 2018.

Carberry, L., Roesler, C., and Drapeau, S.: Correcting in situ chlorophyll fluorescence time-series observations for nonphotochemical quenching and tidal variability reveals nonconservative phytoplankton variability in coastal waters, Limnology and Oceanography: Methods, 17, 462–473, 2019.

Carr, M.-E., Friedrichs, M. A., Schmeltz, M., Aita, M. N., Antoine, D., Arrigo, K. R., Asanuma, I., Aumont, O., Barber, R., Behrenfeld, M., et al.: A comparison of global estimates of marine primary production from ocean color, Deep Sea Research Part II: Topical Studies in Oceanography, 53, 741–770, 2006.

Carr, M. R.: Modelling the attenuation of broad band light down a water column, Journal of the Royal Statistical Society: Series D (The Statistician), 35, 325–333, 1986.

Chai, F., Johnson, K. S., Claustre, H., Xing, X., Wang, Y., Boss, E., Riser, S., Fennel, K., Schofield, O., and Sutton, A.: Monitoring ocean biogeochemistry with autonomous platforms, Nature Reviews Earth & Environment, 1, 315–326, 2020.

Cullen, J. J.: Subsurface chlorophyll maximum layers: enduring enigma or mystery solved?, Annual Reviews, 2015.

Fernand, L., Weston, K., Morris, T., Greenwood, N., Brown, J., and Jickells, T.: The contribution of the deep chlorophyll maximum to primary production in a seasonally stratified shelf sea, the North Sea, Biogeochemistry, 113, 153–166, 2013.

Ferreira, J. G., Andersen, J. H., Borja, A., Bricker, S. B., Camp, J., Da Silva, M. C., Garcés, E., Heiskanen, A.-S., Humborg, C., Ignatiades, L., et al.: Overview of eutrophication indicators to assess environmental status within the European Marine Strategy Framework Directive, Estuarine Coastal and Shelf Science, 93, 117–131, 2011.

Field, C. B., Behrenfeld, M. J., Randerson, J. T., and Falkowski, P.: Primary production of the biosphere: integrating terrestrial and oceanic components, Science, 281, 237–240, 1998.

Frouin, R., Lingner, D. W., Gautier, C., Baker, K. S., and Smith, R. C.: A simple analytical formula to compute clear sky total and photosynthetically available solar irradiance at the ocean surface, Journal of Geophysical Research: Oceans, 94, 9731–9742, 1989.

Gordon, H. R. and Clark, D. K.: Remote sensing optical properties of a stratified ocean: an improved interpretation, Applied Optics, 19, 3428–3430, 1980.

Gregg, W. W. and Carder, K. L.: A simple spectral solar irradiance model for cloudless maritime atmospheres, Limnology and Oceanography, 35, 1657–1675, 1990.

Hansen, C., Kvaleberg, E., and Samuelsen, A.: Anticyclonic eddies in the Norwegian Sea; their generation, evolution and impact on primary production, Deep Sea Research Part I: Oceanographic Research Papers, 57, 1079–1091, 2010.

425 Hemsley, V. S., Smyth, T. J., Martin, A. P., Frajka-Williams, E., Thompson, A. F., Damerell, G., and Painter, S. C.: Estimating oceanic primary production using vertical irradiance and chlorophyll profiles from ocean gliders in the North Atlantic, Environmental Science & Technology, 49, 11 612–11 621, 2015.

Holte, J. and Talley, L.: A new algorithm for finding mixed layer depths with applications to Argo data and Subantarctic Mode Water formation, Journal of Atmospheric and Oceanic Technology, 26, 1920–1939, 2009.

430 Hu, Z., Tan, Y., Song, X., Zhou, L., Lian, X., Huang, L., and He, Y.: Influence of mesoscale eddies on primary production in the South China Sea during spring inter-monsoon period, Acta Oceanologica Sinica, 33, 118–128, 2014.

Jacox, M. G., Edwards, C. A., Kahru, M., Rudnick, D. L., and Kudela, R. M.: The potential for improving remote primary productivity estimates through subsurface chlorophyll and irradiance measurement, Deep Sea Research Part II: Topical Studies in Oceanography, 112, 107–116, 2015.

435 Joint, I. and Pomroy, A.: Phytoplankton biomass and production in the southern North Sea, Marine Ecology-Progress Series, 99, 169–169, 1993.

Joint, I., Groom, S. B., Wollast, R., Chou, L., Tilstone, G. H., Figueiras, F. G., Loijens, M., and Smyth, T. J.: The response of phytoplankton production to periodic upwelling and relaxation events at the Iberian shelf break: estimates by the 14C method and by satellite remote sensing, Journal of Marine Systems, 32, 219–238, 2002.

440 Kiefer, D.: Chlorophyll a fluorescence in marine centric diatoms: responses of chloroplasts to light and nutrient stress, Marine Biology, 23, 39–46, 1973.

Kulk, G., Platt, T., Dingle, J., Jackson, T., Jönsson, B. F., Bouman, H. A., Babin, M., Brewin, R. J., Doblin, M., Estrada, M., et al.: Primary production, an index of climate change in the ocean: satellite-based estimates over two decades, Remote Sensing, 12, 826, 2020.

Le Traon, P. Y., Reppucci, A., Alvarez Fanjul, E., Aouf, L., Behrens, A., Belmonte, M., Bentamy, A., Bertino, L., Brando, V. E., Kreiner,
445 M. B., et al.: From observation to information and users: the Copernicus Marine Service perspective, Frontiers in Marine Science, 6, 234, 2019.

Lee, Z., Weidemann, A., Kindle, J., Arnone, R., Carder, K. L., and Davis, C.: Euphotic zone depth: Its derivation and implication to ocean-color remote sensing, Journal of Geophysical Research: Oceans, 112, 2007.

Liblik, T., Karstensen, J., Testor, P., Alenius, P., Hayes, D., Ruiz, S., Heywood, K., Pouliquen, S., Mortier, L., and Mauri, E.: Potential for an
450 underwater glider component as part of the Global Ocean Observing System, Methods in Oceanography, 17, 50–82, 2016.

Loveday, B. R. and Smyth, T.: An Alternative Framework to Assess Marine Ecosystem Functioning in Shelf Seas (AlterEco) Primary productivity estimates derived from ocean glider in situ sensors and photosynthetically available radiation estimates from in situ and satellite data between November 2017 and May 2019 in the North Sea, British Oceanographic Data Centre, National Oceanography Centre, NERC, UK, https://www.bodc.ac.uk/data/published_data_library/catalogue/10.5285/b58e83f0-d8f3-4a83-e053-6c86abc0bbb5/,
455 2020.

Mignot, A., Claustre, H., Uitz, J., Poteau, A., d'Ortenzio, F., and Xing, X.: Understanding the seasonal dynamics of phytoplankton biomass and the deep chlorophyll maximum in oligotrophic environments: A Bio-Argo float investigation, Global Biogeochemical Cycles, 28, 856–876, 2014.

Miller, P.: Composite front maps for improved visibility of dynamic sea-surface features on cloudy SeaWiFS and AVHRR data, Journal of
460 Marine Systems, 78, 327–336, 2009.

Moll, A.: Regional distribution of primary production in the North Sea simulated by a three-dimensional model, Journal of Marine Systems, 16, 151–170, 1998.

Morel, A.: Light and marine photosynthesis: a spectral model with geochemical and climatological implications, Progress in Oceanography, 26, 263–306, 1991.

465   Morel, A. and Berthon, J.-F.: Surface pigments, algal biomass profiles, and potential production of the euphotic layer: Relationships reinvestigated in view of remote-sensing applications, Limnology and Oceanography, 34, 1545–1562, 1989.

Morel, A. and Maritorena, S.: Bio-optical properties of oceanic waters: A reappraisal, Journal of Geophysical Research: Oceans, 106, 7163–7180, 2001.

Nightingale, P. D., Malin, G., Law, C. S., Watson, A. J., Liss, P. S., Liddicoat, M. I., Boutin, J., and Upstill-Goddard, R. C.: In situ evaluation
470   of air-sea gas exchange parameterizations using novel conservative and volatile tracers, Global Biogeochemical Cycles, 14, 373–387, 2000.

Olita, A., Capet, A., Claret, M., Mahadevan, A., Poulain, P. M., Ribotti, A., Ruiz, S., Tintoré, J., Tovar-Sánchez, A., and Pascual, A.: Frontal dynamics boost primary production in the summer stratified Mediterranean Sea, Ocean Dynamics, 67, 767–782, 2017.

Parekh, P., Follows, M. J., Dutkiewicz, S., and Ito, T.: Physical and biological regulation of the soft tissue carbon pump, Paleoceanography,
475   21, 2006.

Queste, B. Y., Fernand, L., Jickells, T. D., Heywood, K. J., and Hind, A. J.: Drivers of summer oxygen depletion in the central North Sea, Biogeosciences, 13, 1209–1222, 2016.

Reed, D. C., Rassweiler, A., Carr, M. H., Cavanaugh, K. C., Malone, D. P., and Siegel, D. A.: Wave disturbance overwhelms top-down and bottom-up control of primary production in California kelp forests, Ecology, 92, 2108–2116, 2011.

480   Robinson, C., Tilstone, G. H., Rees, A. P., Smyth, T. J., Fishwick, J. R., Tarran, G. A., Luz, B., Barkan, E., and David, E.: Comparison of in vitro and in situ plankton production determinations, Aquatic Microbial Ecology, 54, 13–34, 2009.

Roemmich, D., Alford, M., Claustre, H., Johnson, K., King, B., Moum, J., et al.: On the future of Argo: an enhanced global array of physical and biogeochemical sensing floats. Front, Mar. Sci, 6, 439, 2019.

Salomons, W., Bayne, B. L., Duursma, E. K., and Förstner, U.: Pollution of the North Sea: an assessment, Springer Science & Business
485   Media, 2012.

Sathyendranath, S., Brewin, R. J., Brockmann, C., Brotas, V., Calton, B., Chuprin, A., Cipollini, P., Couto, A. B., Dingle, J., Doerffer, R., et al.: An ocean-colour time series for use in climate studies: the experience of the ocean-colour climate change initiative (OC-CCI), Sensors, 19, 4285, 2019.

Saulquin, B., Hamdi, A., Gohin, F., Populus, J., Mangin, A., and d'Andon, O. F.: Estimation of the diffuse attenuation coefficient KdPAR
490   using MERIS and application to seabed habitat mapping, Remote Sensing of Environment, 128, 224–233, 2013.

Sauzède, R., Claustre, H., Jamet, C., Uitz, J., Ras, J., Mignot, A., and D'Ortenzio, F.: Retrieving the vertical distribution of chlorophyll a concentration and phytoplankton community composition from in situ fluorescence profiles: A method based on a neural network with potential for global-scale applications, Journal of Geophysical Research: Oceans, 120, 451–470, 2015.

Sauzède, R., Claustre, H., Uitz, J., Jamet, C., Dall'Olmo, G., d'Ortenzio, F., Gentili, B., Poteau, A., and Schmechtig, C.: A neural network-
495   based method for merging ocean color and Argo data to extend surface bio-optical properties to depth: Retrieval of the particulate backscattering coefficient, Journal of Geophysical Research: Oceans, 121, 2552–2571, 2016.

Skákala, J., Ford, D., Bruggeman, J., Hull, T., Kaiser, J., King, R. R., Loveday, B., Palmer, M. R., Smyth, T., Williams, C. A., et al.: Towards a multi-platform assimilative system for North Sea biogeochemistry, Journal of Geophysical Research: Oceans, 126, e2020JC016 649, 2021.

500 Smith, R. N., Schwager, M., Smith, S. L., Jones, B. H., Rus, D., and Sukhatme, G. S.: Persistent ocean monitoring with underwater gliders: Adapting sampling resolution, Journal of Field Robotics, 28, 714–741, 2011.

Smyth, T., Fishwick, J., Gallienne, C., Stephens, J., and Bale, A.: Technology, design, and operation of an autonomous buoy system in the western English Channel, Journal of Atmospheric and Oceanic Technology, 27, 2056–2064, 2010a.

Smyth, T. J., Fishwick, J. R., Al-Moosawi, L., Cummings, D. G., Harris, C., Kitidis, V., Rees, A., Martinez-Vicente, V., and Woodward,
505 E. M.: A broad spatio-temporal view of the Western English Channel observatory, Journal of Plankton Research, 32, 585–601, 2010b.

Swart, S., Thomalla, S. J., and Monteiro, P. M.: The seasonal cycle of mixed layer dynamics and phytoplankton biomass in the Sub-Antarctic Zone: A high-resolution glider experiment, Journal of Marine Systems, 147, 103–115, 2015.

Taylor, J. R. and Ferrari, R.: Ocean fronts trigger high latitude phytoplankton blooms, Geophysical Research Letters, 38, 2011.

Thomalla, S. J., Racault, M.-F., Swart, S., and Monteiro, P. M.: High-resolution view of the spring bloom initiation and net community
510 production in the Subantarctic Southern Ocean using glider data, ICES Journal of Marine Science, 72, 1999–2020, 2015.

Thomalla, S. J., Moutier, W., Ryan-Keogh, T. J., Gregor, L., and Schütt, J.: An optimized method for correcting fluorescence quenching using optical backscattering on autonomous platforms, Limnology and Oceanography: Methods, 16, 132–144, 2018.

van Beusekom, J. and Diel-Christiansen, S.: A synthesis of phyto and zooplankton dynamics in the North Sea environment, WWF reports, 1994.

515 Varela, R. A., Cruzado, A., and Gabaldón, J. E.: Modelling primary production in the North Sea using the European regional seas ecosystem model, Netherlands Journal of Sea Research, 33, 337–361, 1995.

Wanninkhof, R.: Relationship between wind speed and gas exchange over the ocean, Journal of Geophysical Research: Oceans, 97, 7373–7382, 1992.

Xing, X., Claustre, H., Blain, S., d'Ortenzio, F., Antoine, D., Ras, J., and Guinet, C.: Quenching correction for in vivo chlorophyll fluo-
520 rescence acquired by autonomous platforms: A case study with instrumented elephant seals in the Kerguelen region (Southern Ocean), Limnology and Oceanography: Methods, 10, 483–495, 2012.

Zhao, C., Daewel, U., and Schrum, C.: Tidal impacts on primary production in the North Sea, Earth System Dynamics, 10, 287–317, 2019.
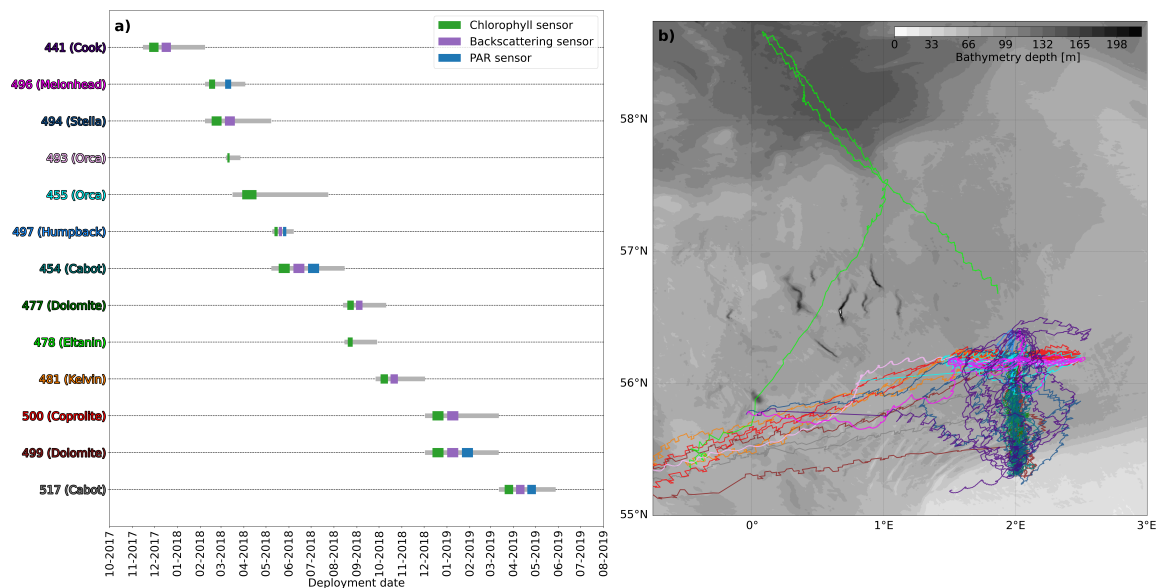
Figure 1. a) Overview of the AlterEco glider deployment schedule and sensor payloads relevant to primary production calculations. b) Trajectories of glider deployments overlaid on the General Bathymetric Chart of the Oceans (GEBCO) 2020 15" bathymetry for the North Sea. Track colours match the respectively coloured glider name from panel (a) (and with Figure 8), with warmer track colours corresponding to later deployments.
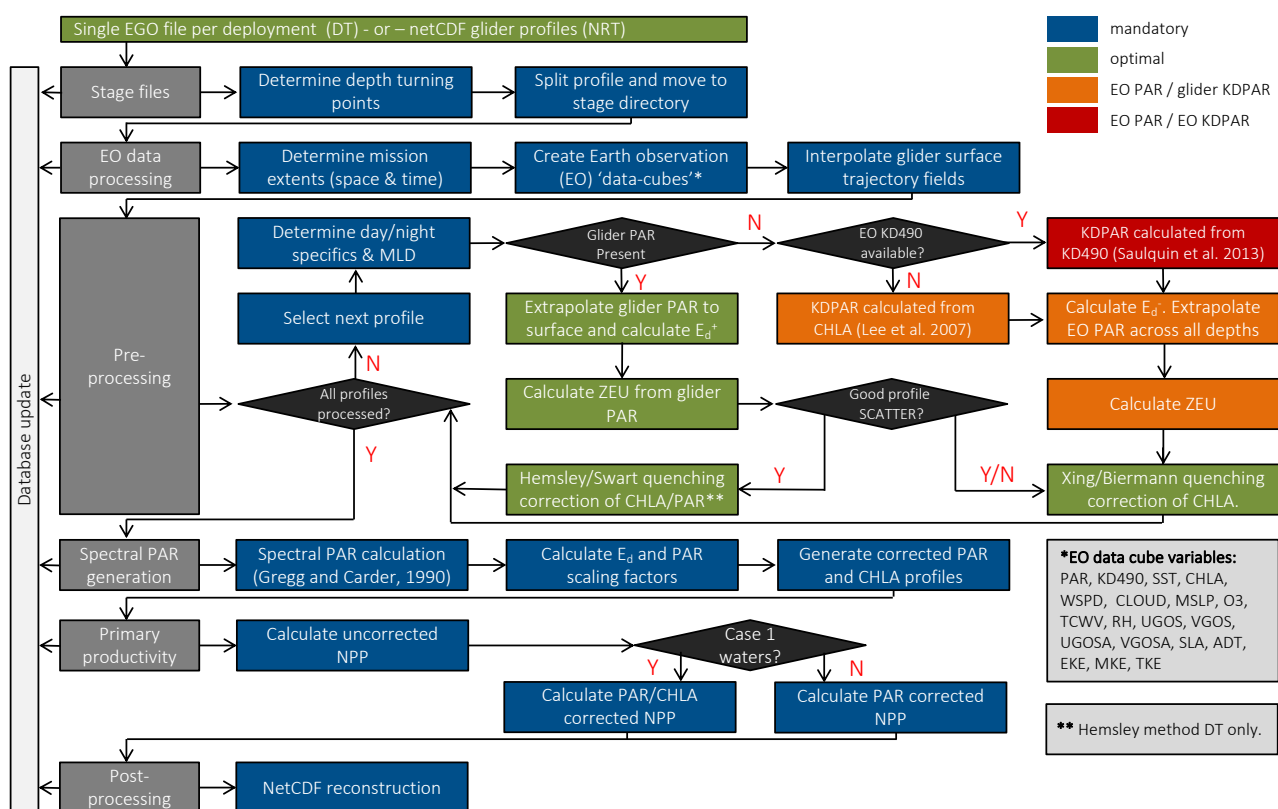
Figure 2. Schematic overview of the glider-based primary production processing chain. Blue boxes indicate mandatory steps; Green, orange and red boxes indicate processing options in order of decreasing preference. The light grey inset box describes the Earth observation variables that are interpolated onto a glider's path.
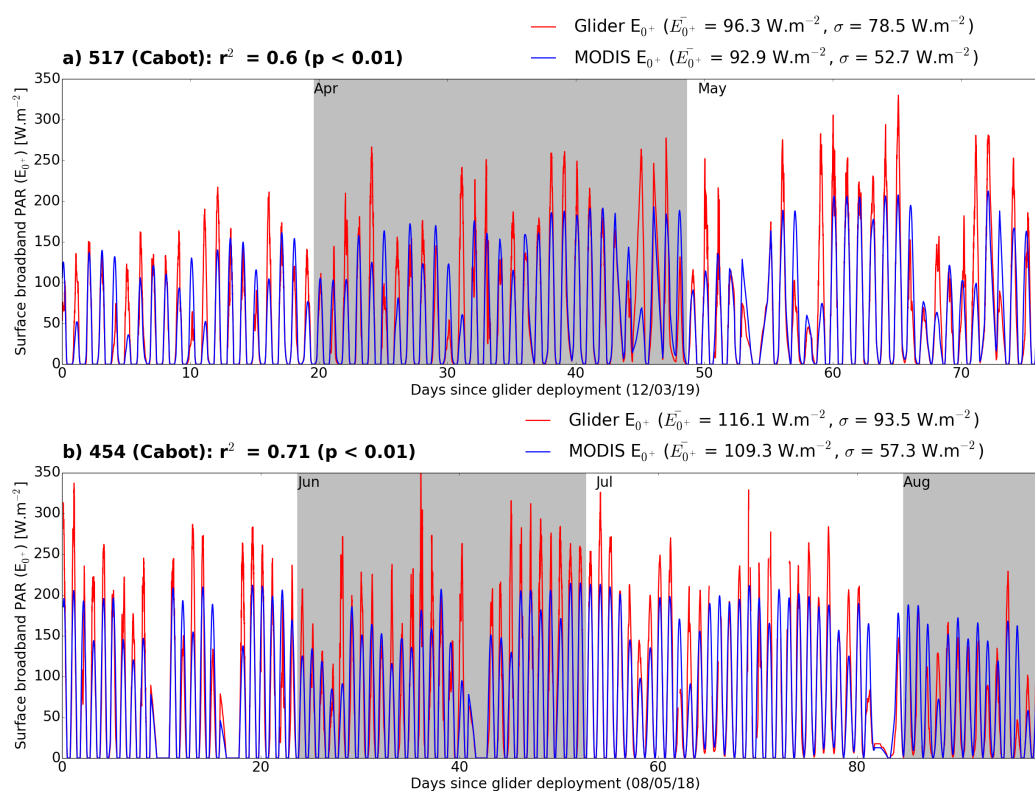
Figure 3. Comparison of glider and MODIS based surface broadband PAR (E0$^+$) values. Red and blue traces show the 10-profile smoothed PAR for the glider and interpolated MODIS products, respectively. All statistics (r^2, μ, σ) are based on the valid, unsmoothed time-series data, for day-time profiles only.
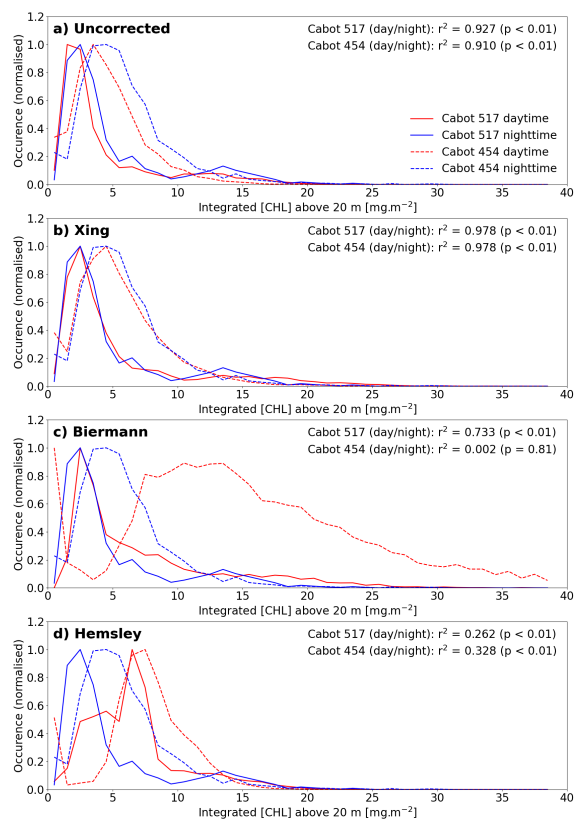
Figure 4. The effects of the implementation of different quenching mechanisms on the distribution of the integrated [Chl-a] in the top 20 m for Cabot deployments 454 (dashed lines) and 517 (solid lines). Panel a) shows the distribution of day-time (red) and night time (blue) [Chl-a] in the uncorrected case. Panels b), c) and d) show the effects of implementing the mixed layer depth based correction of Xing et al. (2012), euphotic depth based correction of Biermann et al. (2015), and scattering based correction of Hemsley et al. (2015).
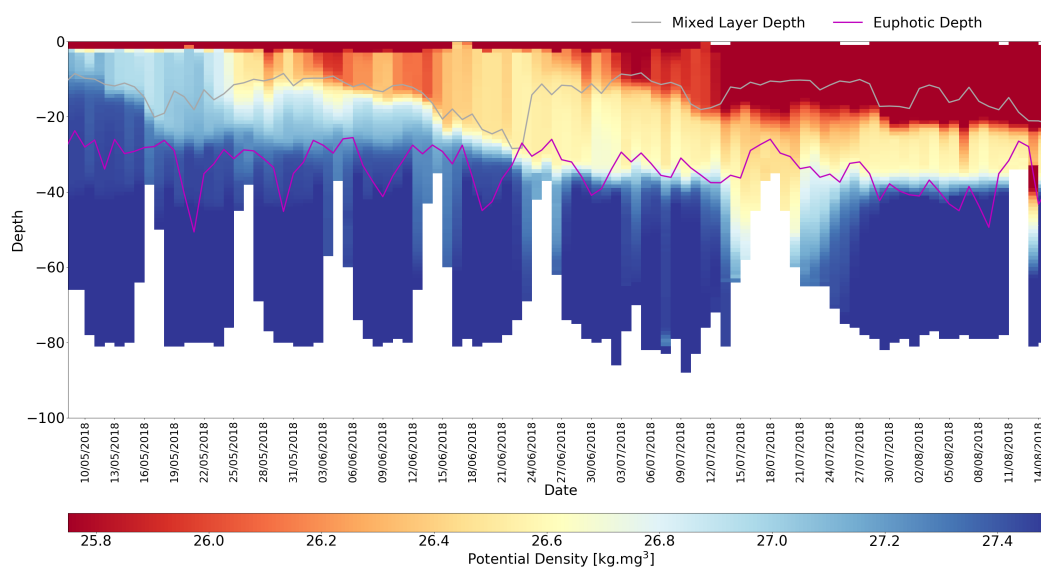
Figure 5. Potential density distribution for time series for 454 (Cabot). Mixed layer depth and euphotic depths are shown by the respective grey and purple traces, which have been smoothed using a 10 profile window. Gaps in the euphotic depth time series correspond to night-time profiles.
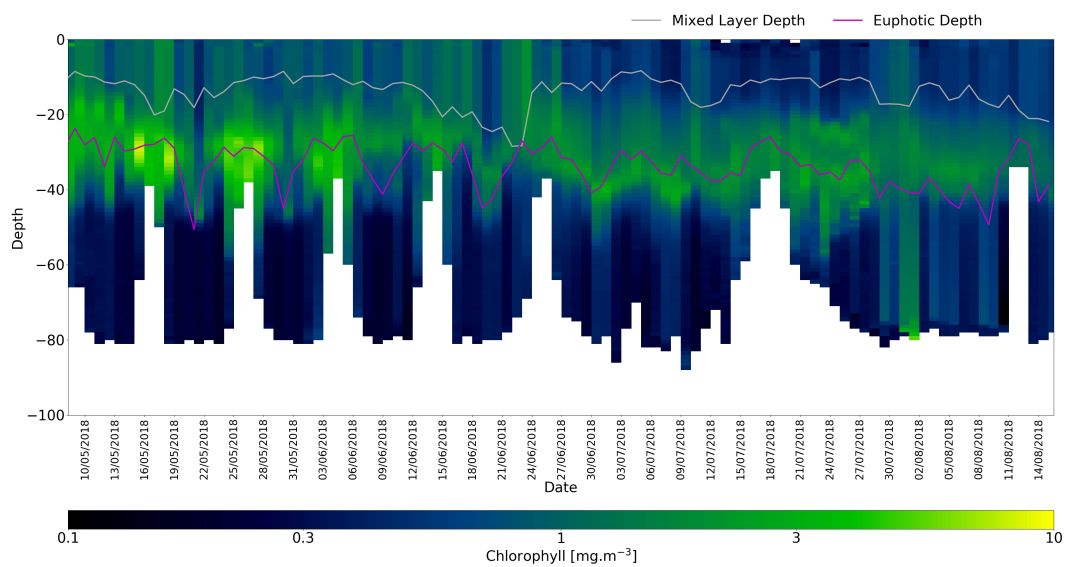
Figure 6. Quenching corrected [Chl-a] time series for 454 (Cabot). The Xing et al. (2012) quenching corrected is applied. Mixed layer depth and euphotic depths are as in figure 5).
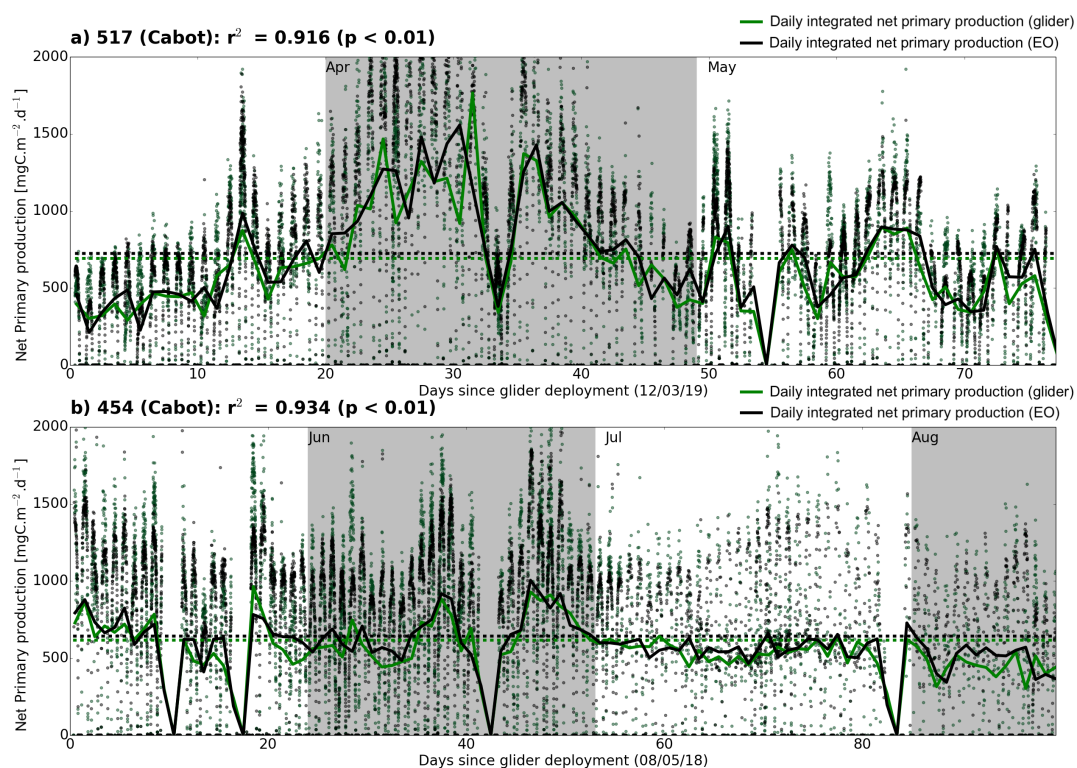
Figure 7. Comparison of net primary production estimates from the in situ based PAR method (green points and traces) and SEO-based PAR method (black points and traces) for glider Cabot for missions a) 517 and b) 454. Points represent the instantaneous measurements taken from individual profiles, with solid traces showing the daily integrated values. Total mean daily values for each mission and method are given by the respective dashed lines. The r^2 statistic is calculated between the individual profile values for the two methods.
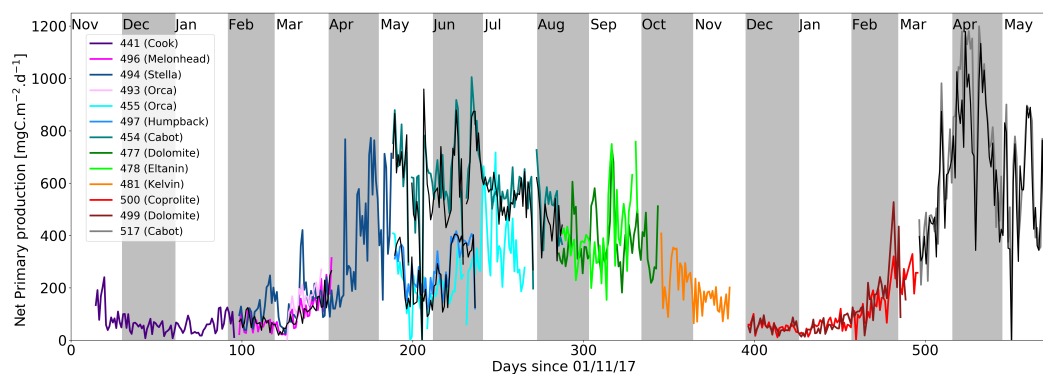
Figure 8. Daily integrated net primary production estimates from all gliders deployed in the AlterEco programme (see table 1). Coloured traces represent each glider mission (matching those used in figure 1), and show the net primary production estimates derived from the SEO-based PAR method. Where in situ PAR sensors were available, a corresponding black trace for that glider mission is also shown.

Table 1. An overview of mission nomenclature. All glider data used in the calculation of primary production is available at https://www.bodc.ac.uk/data/bodc_database/gliders/ and is published under the following dois: 10.5285/b57d215e-065f-7f81-e053-6c86abc01a82 and 10.5285/86429662-97b8-74fa-e053-6c86abc0a97c

Campaign	Platform	Deployment	Glider serial	Processed here
AlterEco1	Fin	439	SG537	No, incompatible sensor load
	Stella	440	unit_436	No, incompatible sensor load
	Cook	441	unit_194	Yes
AlterEco2	Orca	493	SG510	Yes
	Stella	494	unit_436	Yes
	OMG-1	495	unit_352	No, incompatible sensor load
	Melonhead	496	sg620	Yes
AlterEco3	Cabot	454	unit_345	Yes
	Orca	455	SG510	Yes
	Humpback	497	SG579	Yes
	Lyra	486	999	No, incompatible sensor load
AlterEco4	Dolomite	477	unit_305	Yes
	Eltanin	478	SG550	Yes
	Scapa	479	SG602	No, incompatible sensor load
	Lyra	480	999	No, incompatible sensor load
AlterEco5	Kelvin	481	unit_444	Yes
AlterEco6	Dolomite	499	unit_305	Yes
	Coprolite	500	unit_331	Yes
AlterEco7	Ammonite	516	unit_304	No, incompatible sensor load
	Cabot	517	unit_345	Yes
	Scapa	518	SG602	No, incompatible sensor load

Table 2. List of SEO and reanalysis variables used to support glider missions. Bold type variables are derived by the primary production processor.

Description	Provider	Source	Variables
Sea surface topography	CMEMS	SEALEVEL_GLO_PHY_L4_NRT & REP	sea-level anomaly
			absolute dynamic topography
			absolute geostrophic velocities
			geostrophic velocities anomalies
			eddy kinetic energy
			total kinetic energy
			mean kinetic energy
Atmospheric variables	ECMWF	ERA-I	10 m wind speed (u/v)
			total cloud cover
			mean sea level pressure
			$[O_3]$
			[water vapour]
			2 m temperature
			2 m dew point
			wind speed
			relative humidity
Optical variables	NASA	MODIS L3m Daily products	PAR
			K_{d490}
			instantaneous PAR
Ocean tracers	CMEMS	GLOBAL_ANALYSIS_FORECAST_PHY	sea surface temperature
			sea surface salinity
			mixed layer depth
Biogeochemistry	CMEMS	OCEANCOLOUR_GLO_CHL_L3_NRT & REP	[CHLA]
			euphotic depth

Table 3. Variables present in the EGO format netCDF data files. All variables have a single 'time' dimension.

Variable name	Quantity	Units
TIME	time	seconds since 1970-01-01
PROFILE_NUMBER	glider profile number	none
LONGITUDE	longitude	degrees east
LATITUDE	latitude	degrees north
PRESSURE	pressure	decibar
DEPTH	glider depth	m
CHLA	quenching corrected [CHL-a]	mg m^{-3}
MIXED_LAYER_DEPTH	mixed layer depth	m
EUPHOTIC_DEPTH	Euphotic depth (ZEU)	m
EUPHOTIC_DEPTH_FLAG	Euphotic depth method flag	none
DOWNWELLING_PAR	photosynthetically active radiation (PAR)	W m^{-2}
DOWNWELLING_PAR_FLAG	PAR method flag	none
DOWNWELLING_PAR_EO	PAR from satellite Earth observation (SEO)	W m^{-2}
DOWNWELLING_PAR_EO_FLAG	SEO PAR method flag	none
PRIMARY_PRODUCTION	Primary production (PP) from in situ PAR	carbon flux of mg m^{-3} d^{-1}
PRIMARY_PRODUCTION_EO	PP from SEO PAR	carbon flux of mg m^{-3} d^{-1}
DEPTH_INTEGRATED_PRIMARY_PRODUCTION	PP integrated to ZEU	carbon flux of mg m^{-2} d^{-1}
DEPTH........._PRODUCTION_EO	SEO PP integrated to ZEU	carbon flux of mg m^{-2} d^{-1}

Note; DOWNWELLING_PAR_FLAG and DOWNWELLING_PAR_EO_FLAG are equivalent, but are included twice as they are relevant to both of their associated variables.

Table 4. Monthly statistics for SEO-PAR based depth integrated primary production estimates across all glider missions. Values for in situ PAR based depth integrated primary production estimates are given in brackets, where available. All measurements are given in carbon flux, measured in g m^{-2} d^{-1}, unless otherwise specified. The final column gives the mean primary production extracted from v4.2 of the monthly OC-CCI climatology from 01/01/1998 to 31/12/2018 over a box spanning the core of the AlterEco sampling region (1.5^o E to 2.5^o E, 55.25^o N to 56.25^o N).

Month	NPP Mean	NPP Std. deviation	N profiles	OC-CCI NPP Mean*	OC-CCI NPP std. dev.*
January	53	21	8190	64	69
February	138 (70)	139 (23)	9925 (2381)	166	31
March	192 (184)	125 (131)	10868 (5105)	358	79
April	470 (607)	269 (251)	7393 (3336)	617	112
May	391 (416)	157 (158)	9382 (7132)	594	131
June	406 (476)	110 (142)	7951 (5916)	340	73
July	364 (397)	127 (138)	1634 (1498)	303	49
August	334 (344)	83 (74)	3928 (628)	278	58
September	317	91	4165	234	51
October	192	73	2923	177	31
November	134	50	2554	109	55
December	49	16	5276	4	13
Annual	269	199	74189	270	63
Annual (mg m^{-2} d^{-1})	269	199	74189	270	63
Annual (g m^{-2} a^{-1})	98	73	74189	99	23

*Data provided by Plymouth Marine Laboratory, based on Kulk et al. (2020)